International Journal of Applied Earth Observation and Geoinformation 43 (2015) 32–42

Contents lists available at ScienceDirect

International Journal of Applied Earth Observation and Geoinformation

journal homepage: www.elsevier.com/locate/jag

Estimating chlorophyll with thermal and broadband multispectral high resolution imagery from an unmanned aerial system using relevance vector machines for precision agriculture

Manal Elarab[a,b,*], Andres M Ticlavilca[b], Alfonso F. Torres-Rua[b], Inga Maslova[c], Mac McKee[a,b]

[a] Civil and Environmental Engineering Department, Utah State University, USA
[b] Utah Water Research Laboratory, Utah State University, USA
[c] American University, Washington D.C., USA

ARTICLE INFO

Article history:
Received 31 October 2014
Accepted 31 March 2015
Available online 17 April 2015

Keywords:
Remote sensing
High spatial resolution imagery
Relevance vector machine
Precision agriculture
Chlorophyll concentration

ABSTRACT

Precision agriculture requires high-resolution information to enable greater precision in the management of inputs to production. Actionable information about crop and field status must be acquired at high spatial resolution and at a temporal frequency appropriate for timely responses. In this study, high spatial resolution imagery was obtained through the use of a small, unmanned aerial system called AggieAir™. Simultaneously with the AggieAir flights, intensive ground sampling for plant chlorophyll was conducted at precisely determined locations. This study reports the application of a relevance vector machine coupled with cross validation and backward elimination to a dataset composed of reflectance from high-resolution multi-spectral imagery (VIS–NIR), thermal infrared imagery, and vegetative indices, in conjunction with in situ SPAD measurements from which chlorophyll concentrations were derived, to estimate chlorophyll concentration from remotely sensed data at 15-cm resolution. The results indicate that a relevance vector machine with a thin plate spline kernel type and kernel width of 5.4, having LAI, NDVI, thermal and red bands as the selected set of inputs, can be used to spatially estimate chlorophyll concentration with a root-mean-squared-error of 5.31 $\mu g\,cm^{-2}$, efficiency of 0.76, and 9 relevance vectors.

1. Introduction

Increasing world population levels will bring increased demand for food, water, and agricultural inputs. Various agricultural farming strategies are being reevaluated to determine how to improve food production, minimize environmental impact, and reduce costs. Among many, Precision Agriculture (PA) has evolved as a viable system to improve profitability and productivity (Swinton and Lowenberg-DeBoer, 1998; Lambert and Lowenberg-De Boer, 2000; Daberkow et al., 2000). PA is a process of finely adjusting agricultural inputs (e.g., water, nutrients) and in-field practices (e.g., irrigation, fertilization), through the use of site-specific information and spatial imagery, to improve measures of agricultural productivity (e.g., yield, net farm income) (Pierce and Nowak, 1999).

Use of spatial imagery in agriculture has been the focus of many studies for the past five decades (MacDonald and Hall, 1980; Bauer, 1985; Idso et al., 1977; Benedetti and Rossini, 1993; Shanahan et al., 2001; Stone et al., 1996; Mathur and Foody, 2008; Franke and Menz, 2007), requiring increased investments in relevant research and technologies (Schellberg et al., 2008) that indicate that remote sensing can be a valuable tool to enhance precision agriculture (Lamb and Brown, 2001; Haboudane et al., 2002; Seelan et al., 2003). However, remote sensing has yet to reach its full capability in PA applications. Lack of fine spatial resolution and near real-time data, compounded by high costs, has hindered remote sensing applications at the field scale (Brisco et al., 1998; Liaghat and Balasundram, 2010; Moran et al., 1997; Kalluri et al., 2002). Thirty years ago, Jackson (Jackson, 1984) envisioned an autonomous remote sensing platform that could overcome most of the limitations; this is becoming a reality with the introduction of affordable unmanned aerial systems (UAS). UAS, a potential substitute for satellite-based remote sensing, are gaining attention and recognition in the scientific community as a potential technology that can generate

* Corresponding author at: Utah Water Research Laboratory, Utah State University, USA. Tel.: +1 435 754 9299; fax: +1 435 797 3663.
E-mail address: alarabmanal@gmail.com (M. Elarab).

http://dx.doi.org/10.1016/j.jag.2015.03.017

high spatial resolution imagery (<1 m) and at a temporal frequency appropriate for timely responses in the production of actionable information about crop and field status. One such UAS, named AggieAir™, was developed by the Utah Water Research Laboratory (UWRL) at Utah State University. AggieAir is designed to carry camera payloads to acquire high resolution, georeferenced aerial imagery to be used in various water, natural resources, and agricultural applications, including PA. AggieAir holds three sensors: sensors one and two are consumer-grade cameras (personal point-and-click cameras) that capture imagery, depending on flight elevation above ground, of 6–25 cm resolution in the visible (red, green, blue spectrum) and near – infrared spectrum, respectively; sensor three is a microbolometer thermal camera that captures images of 30–150 cm resolution in the thermal infrared spectrum. The three sensors are ideal because of their small size, light weight, low-cost, and high resolution. The use of high-resolution imagery (<1 m) can potentially improve the ability to evaluate the spatial dynamics of chlorophyll and detect its temporal variation. In this study, the use of multispectral VIS-NIR-thermal high-resolution imagery is investigated as a tool to estimate plant chlorophyll concentration to provide time-critical information for PA.

Chlorophyll concentration, measured in mass per unit leaf area ($\mu g\,cm^{-2}$), is an important biophysical parameters retrievable from reflectance data. Chlorophyll is a vital pigment primarily responsible for harvesting light energy used in photosynthesis (Sims and Gamon, 2002; Evans, 1989; Niinemets and Tenhunen, 1997) and is therefore an excellent indicator of a crop's overall physiological status (Evans, 1989; Yoder and Pettigrew-Crosby, 1995) stress or disease (Zarco-Tejada et al., 2004; Peñuelas and Filella, 1998; Chaerle and Van Der Straeten, 2000), and yield predictions (Dawson et al., 2003; Gitelson et al., 2006). Chlorophyll can potentially provide an assessment of leaf nitrogen, an essential plant nutrient, due to the close relationship between leaf chlorophyll and leaf nitrogen (Daughtry et al., 2000; Moran et al., 2000; Wood et al., 1992). Chlorophyll concentration varies with vegetation growth, thus estimating chlorophyll across the field at different growth stages could offer the farmer time- and location-specific critical information ideal for assisting decision makers in monitoring their crops and managing farming activities to achieve maximum production.

Several leaf scale studies have focused on estimating chlorophyll concentration from VIS–NIR reflectance data. These studies indicate that the green and far-red regions of the visible spectrum are sensitive to variations in chlorophyll concentrations (Kim, 1994; Datt, 1999; Gitelson and Merzlyak, 1994; Zarco-Tejada et al., 2001; Demarez and Gastellu-Etchegorry, 2000). Various successful indices have been formulated to estimate chlorophyll concentration (Bonge and Leblanc, 2001; Le Maire et al., 2004; Haboudane et al., 2002). Some of these indices are ratios of reflectance in individual narrow visible wavebands (Blackburn, 1998; Carter and Spiering, 2002) or ratios of reflectance in VIS and NIR (Gitelson et al., 1996), while others are red edge reflectance ratio indices (Gitelson and Merzlyak, 1994; Zarco-Tejada and Miller, 1999; Kim et al., 1994) or first and second derivatives of reflectance spectra (Miller et al., 1990). Composites of indices have been developed (Haboudane et al., 2002) in an attempt to correct for distortions in the reflectance data caused by soil background effect and canopy architecture. Detailed discussions and thorough reviews concerning appropriate optimal wavelengths and various chlorophyll indices can be found in the literature (Haboudane et al., 2004; Bonge and Leblanc, 2001). However, most of the studies have had low spatial and coarse spectral resolution characteristics; therefore, the applicability of those indices to high spatial resolution airborne data cannot be evaluated. Regarding thermal imagery, it was mainly explored when information on plant water status was in question, for example when screening drought tolerance genotypes (Blum et al., 1982), detecting crop water stress levels (Bernie et al., 2009), estimating soil moisture and evapotranspiration (Jackson et al., 1981; Wallace et al., 2012; Hassan Esfahani et al., 2014a). However, TIR data haven't been investigated in estimating chlorophyll yet. Exploring thermal data in this study is rationalized by the close relationship between heat stress and the photosynthetic capacity of the leaves (Raison et al., 1982; Sharkey, 2005) and consequently the chlorophyll concentration. The mechanism by which moderate heat stress reduces photosynthetic capacity has been debated since the eighties where researchers attributed the photosynthesis inhibition to different factors such as the impairment of electron transport activity or the inactivation of Rubisco (Berry and Bjorkman, 1980; Murakami et al., 2000; Weis, 1981; Salvucci and Crafts-Brandner, 2004).

Estimating chlorophyll at a canopy level from optical remotely sensed data can generally be carried out by several methodologies. The simplest methodology that is widely accepted is the empirical method, such as those based on vegetation indices (Johnson et al., 1994). Nevertheless, indices generated in this context are inclined to unstable performance when applied to images that differ from the designed method (Verrelst et al., 2010). Physical behavior based methods are another approach to formulating estimates from remotely sensed data. This method is based on physical laws that describe the transfer and interaction of radiation within the atmospheric column and canopy, such as radiative transfer models (RT) (Myneni et al., 1995). This approach has become more promising with advances in atmospheric radiative transfer modeling. The biggest drawback for such a model is that it requires site-specific information for proper model parameterization, which is not always available. As a result, methods based on vegetation indices or physical models may be either too simple or too complex to deliver accurate estimates (Baret and Buis, 2008). Several books and published papers have reviewed these methodologies and highlighted the advantages and disadvantages associated with the complexity of the modeling approach selected, and the degree of general or local applicability of the methodology in remote sensing (Baret and Buis, 2008; Zarco-Tejada et al., 2001).

Considerable research has been carried out to explore advanced computational methods that are both accurate and robust. Machine learning regression algorithms present a potential approach for generating adaptive, robust, and, once trained, fast estimates (Hastie et al., 2009; Knudby et al., 2010). Recent studies have demonstrated successful performance of a very well-known machine learning algorithm in estimating biophysical parameters using neural network models (Cipollini et al., 2001; De Martino et al., 2002; Verrelst et al., 2012; González Vilas et al., 2011; Hassan Esfahani et al., 2014b). In recent studies, neural networks are being replaced by more advanced regression-based methods that are simpler to calibrate, like support vector machines (SVM) (Moser and Serpico, 2009; Camps-Valls et al., 2006; Pal and Mather, 2005) and relevance vector machines (RVM) (Camps-Valls et al., 2006b). SVMs have been widely used in various remote sensing applications; nevertheless, their large computational complexity is a major drawback. This complexity of SVM models is due to their liberal use of basis functions that typically grow linearly with the size of the training set (Tipping, 2001). Studies have shown that the behavior of relevance vector machines (RVM) is often superior to that of SVMs (Demir and Erturk, 2007). The results given by Tipping (2001) demonstrated that the RVM has a comparable generalization performance to the SVM, while requiring dramatically fewer kernel functions or model terms. RVM, is a statistical learning method proposed by Tipping in 2001 (Tipping, 2001), constitutes a Bayesian approximation for solving nonlinear regression models and is often used for classification and pattern recognition. RVMs offer excellent sparseness characteristics, are robust, and can produce probabilistic outputs that permit the capture of uncertainty in the predictions (Gómez-Chova et al., 2011; Thayananthan et al., 2008).

The main purposes of this study were to: (1) introduce AggieAir as a successful tool for use in precision agriculture, (2) explore the use of VIS, NIR and TIR in estimating chlorophyll concentration, and (3) use RVM algorithms to formulate spatially distributed chlorophyll concentration estimates.

2. Material and methods

2.1. Relevance vector machine (RVM)

This section presents a brief description of RVMs relevant to this study. Tipping introduced the relevance vector machine in 2001. The RVM was developed with a Bayesian framework to find sparse solutions in classification and regression studies based on acquiring relevance vectors and weights by maximizing a marginal likelihood. In RVM regression models, the weight of each input is governed by a set of hyperparameters that describe posterior distribution of the weights and are estimated iteratively during the machine learning training step (Tipping, 2001). This paper adopts the RVM introduced by Tipping (Tipping, 2004), which resembles the 2001 model. The main feature in the 2004 model is that the inferred predictors are even sparser, with relatively few relevance vectors. This model also offers good generalization performance (Yuan et al., 2007).

To build the model, input–output vector pairs $\{x_i, y_i\}_{i=1}^{N}$ are sampled from a data set of N input vectors $\{X_n\}_{n=1}^{N}$ with corresponding N output values $\{Y_n\}_{n=1}^{N}$. From these vector paired data, we generate a training data subset from which the model learns the dependence between inputs and the output target, with the purpose of making accurate predictions of y for previously unseen values of x shown in Eq. (1):

$$y = w\Phi(x) + \epsilon \tag{1}$$

where w is a vector of weight parameters, $\Phi(x) = [1, f(x, x_1), \ldots\ldots, f(x, x_N)]^T$ is a design matrix of $N+1$ vectors of kernel basis functions f, ϵ is the error that for algorithmic simplicity is assumed to be zero-mean Gaussian with variance σ^2.

The kernel or basis function, is a method that detects embedded patterns in the data by transforming or extending linear algorithms into non-linear ones. Kernel methods map the data into higher dimensional spaces to increase the computational power of the machine (Souza, 2010; Genton, 2002; Vapnik, 2000; Cristianini and Shawe-Taylor, 2000). Kernel functions could be linear, polynomial and Gaussian kernel. However, choosing the most appropriate one highly depends on the nature of the relationship between the inputs and outputs. Six kernel types, f, were considered: Gauss, Laplace, spline, Cauchy, thin plate spline (tps), and bubble (Bachour et al., 2014; Torres et al., 2011; Ticlavilca et al., 2013). The process of selecting the kernel type in this paper was conducted by trial and error.

The Gaussian likelihood of the data set can be written as in Eq. (2):

$$p(y|w, \sigma^2) = (2\pi)^{-N/2}\sigma^{-N}\exp\left\{-\frac{\|y - w\Phi\|^2}{2\sigma^2}\right\} \tag{2}$$

One of the classic approaches to estimating the parameters w and σ^2 in Eq. (2) is using the method of maximum likelihood. However, with many parameters used as training observations, the maximum likelihood estimation would lead to severe overfitting (Tipping, 2004). To overcome this complexity, Tipping (2001) proposed adding a "prior" to constrain the selection of parameters by defining an explicit zero-mean Gaussian prior probability distribution over them as shown in Eq. (3):

$$p(w|\alpha) = (2\pi)^{-M/2}\prod_{m=1}^{M}\alpha_m^{1/2}\exp\left(-\frac{\alpha_m w_m^2}{2}\right) \tag{3}$$

where M is the number of independent hyperparameters $\alpha = (\alpha_1, \ldots, \alpha_M)^T$. Each α is associated independently with every weight to moderate the strength of the prior and provide the sparsity of the model (Tipping, 2001). How far each weight is allowed to deviate from zero is controlled by the hyperparameter vectors (Yuan et al., 2007). Consequently, using Bayes' posterior inference, the posterior over W could be computed as shown in Eq. (4):

$$p(w|y, \alpha, \sigma^2) = \frac{p(y|w, \sigma^2)p(w|\alpha)}{p(y|\alpha, \sigma^2)} \tag{4}$$

Here, $p(y|\alpha, \sigma^2)$ is the normalizing factor; $p(y|w, \sigma^2)$ and $p(w|\alpha)$ are both Gaussian priors, so the posterior is also Gaussian with $p(w|y, \alpha, \sigma^2) \sim N(w|\mu, \Sigma)$. The posterior mean μ and covariance Σ are defined as:

$$\Sigma = (A + \sigma^{-2}\Phi^T\Phi)^{-1} \tag{5}$$ and

$$\mu = \sigma^{-2}\Sigma\Phi^T y \tag{6};$$

where, A is $diag(\alpha_1, \ldots, \alpha_M)$.

A fast marginal likelihood optimization algorithm is used to obtain the optimal set of hyperparameters, α^{opt}. This optimization algorithm uses an efficient sequential addition and deletion of candidate basis functions described by (Tipping and Faul, 2003).

Given an unseen input vector, x^*, the predictive distribution for the corresponding target y^* can be computed. This search for optimal hyperparameters is learned using a type II maximum likelihood method coupled with iterative re-estimation (Tipping, 2001) as shown in Eq. (7):

$$p(y*|y, \alpha^{opt}, (\sigma^{opt})^2) = \int p(y*|w, (\sigma^{opt})^2)p(w|y, \alpha^{opt}, (\sigma^{opt})^2)dw \tag{7}$$

$$=> \quad p(y*|y, \alpha^{opt}, (\sigma^{opt})^2) = N(y*|\mu*, (\sigma*)^2)$$

where $\mu*$ is the predictive mean of the output of the unseen data, x^*, and the posterior mean weight of μ, $\mu* = \mu^T\Phi(x^*)$; and $(\sigma*)^2 = [(\sigma_1^*)^2, \ldots, (\sigma_M^*)^2]^T$ is the predictive variance. This predictive variance is the sum of variances associated with both the noise of the data and the uncertainty in the prediction of the weight parameters (Tipping, 2004). In this optimization process, the vectors from the training set associated with non-zero weights are called the relevance vectors.

The theory behind RVM, mathematical formulation, likelihood maximization, and optimization procedure are discussed in detail in (Tipping, 2004) and (Tipping and Faul, 2003).

2.2. Study area

The field study was carried out in the summer of 2013 on privately owned agricultural land in Scipio, Utah USA (39°14′N 112°6′W) (Fig. 1). The plot, mainly composed of loamy clay soil, was equipped with a center pivot sprinkler for irrigating and fertigating oats (*Avena sativa*). The study area was restricted to the northwest quarter of the center pivot so that samples could be collected within a close time frame relative to the AggieAir flight. AggieAir aircraft were flown four times over the area, covering the entire growth cycle of oats. The flights on 05/16, 06/01, 06/09, and 06/17 reflected the four stages of growth: 10 days after planting, early growth, mid growth and early flowering. Oats were harvested after the fourth flight to be used as forage.

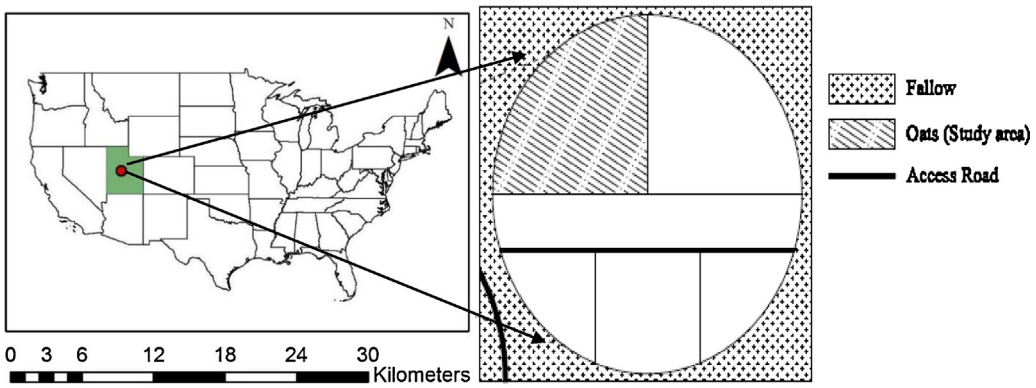

Fig. 1. The location of the study area in Scipio, Utah.

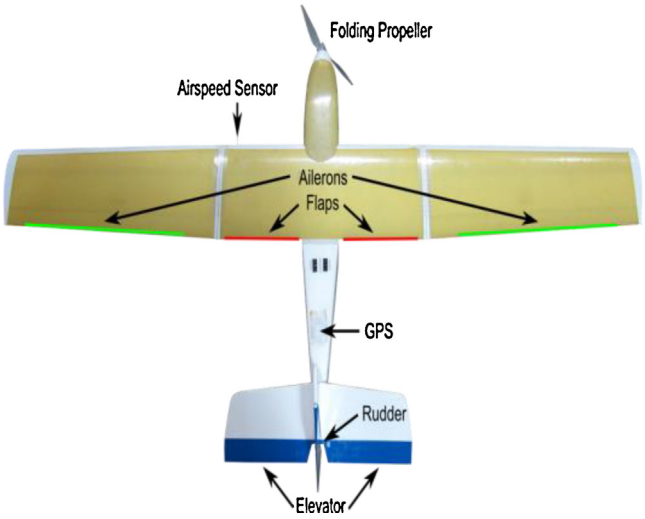

Fig. 2. AggieAir airframe layout.

Table 1
AggieAir UAS specifications.

AggieAir specifications	
Flight duration	45–60 min
Flight altitudes	200–1000 m
Maximum takeoff weight	6.35 kg
VIS–NIR resolution	6–25 cm
Thermal resolution	30–150 cm
Wing span	2.5 m

2.3. Instrumentation: remote sensing platform AggieAir

AggieAir is a UAS designed to carry camera payloads to acquire aerial imagery for PA and other types of applications (Fig. 2). The UAS aircraft is battery powered and equipped with a payload system (which includes three cameras and a computer), avionics, two inertial sensors (a GPS module and an inertial measurement unit), radio controller and flight control. The aircraft is propelled using an electric, brushless motor. It does not require a runway, and can be flown autonomously or manually. In autonomous mode, the aircraft follows a pre-programmed flight plan containing navigation waypoints defined by GPS and altitude. While operational, the payload computer instructs the three cameras to acquire imagery in the VIS, NIR and thermal spectra and records the position and orientation of the aircraft when each image is taken. Table 1 illustrates the UAS specification in more detail.

The VIS camera used in AggieAir is a Canon S-95, with a 10-megapixel CCD sensor and an ISO range of 80–3200. The radiometric resolution of the Canon S-95 is 8-bit color, which means that the digital measurement for a particular pixel in a given spectral band ranges from 0 to 255. The NIR camera is an identical Canon S-95, modified by replacing the manufacturer's optical filter with a Wratten 87 NIR filter that allows NIR wavelengths of 750 nm. The relative spectral responses of the VIS–NIR cameras were not provided by the manufacturers but were obtained using the algorithm provided by (Jiang et al., 2013). The camera VIS–NIR spectral response is shown in (Fig. 3-left). AggieAir also carries a small, low-power, microbolometer thermal camera from Infrared Cameras Inc. (ICI) (Infrared Cameras Incorporated, 2012). The relative spectral response of the thermal camera is shown in (Fig. 3-right).

Following VIS and NIR image acquisition, a two-step processing phase occurs: The first step is image mosaicking and orthorectification. This technique, achieved with EnsoMOSAIC software (MosaicMill users guide, 2009), combines all of the images into one large mosaic and rectifies it into a ground coordinate system. The software generates hundreds of tie-points between overlapping images by using photogrammetric principles in conjunction with image GPS log file data and exterior orientation information from the on-board cameras to refine the estimate of the position and orientation of individual images. The resulting image is an orthorectified digital number mosaic. The second step involves radiometric calibration: the conversion of the digital pixels into a measure of reflectance. This conversion is based on methods adapted from (Neale and Crowther, 1994; Miura and Huete, 2009; Crowther, 1992). The major steps involved in this methodology are the reference panel calibration and solar zenith angle calculations. This method converts raw airborne multispectral data by calculating the ratio of linearly-interpolated reference values from the pre- and post-flight reference panel readings, this is discussed in details in (Zaman et al., 2014; Clemens, 2012). After completing the two-step process, images are geometrically rectified and radiometrically corrected to obtain a four-layer (RGB, NIR) canopy surface reflectance in a single image (Fig. 4).

Thermal imagery processing also requires an initial step of mosaicing and orthorectification similar to the VIS and NIR images. However, the resulting thermal mosaic is composed of brightness temperature in degrees Celsius (±0.1 degrees) instead of digital numbers. Compensating for external disturbance and geometric calibration are also unique challenges associated with the thermal camera (Jensen, 2014), thoroughly explains the methodology of processing thermal maps adopted by the authors.

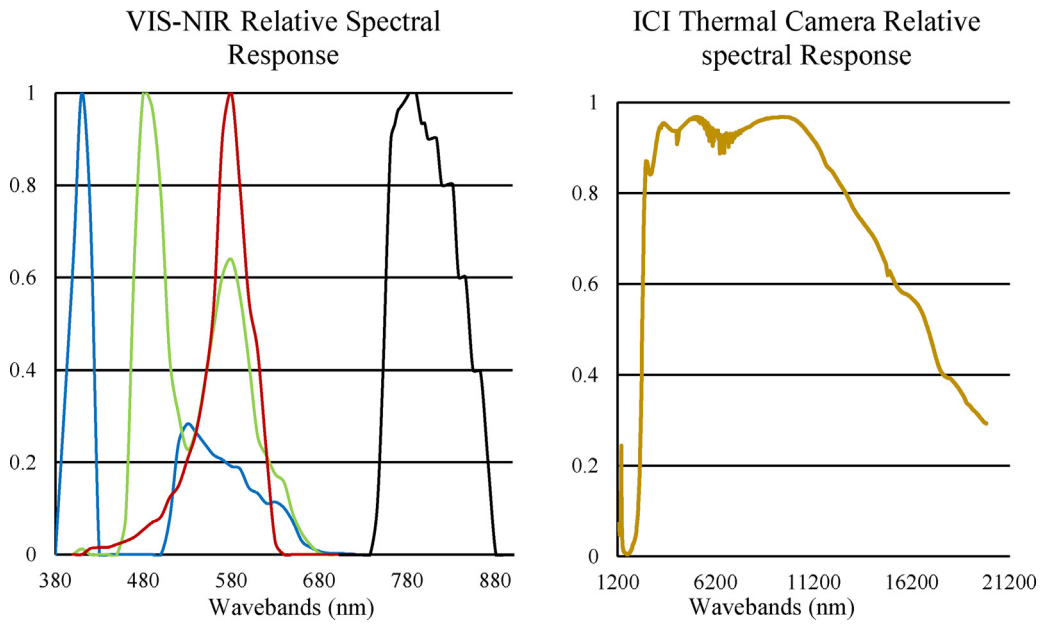

Fig. 3. Relative spectral response of the VIS–NIR (left) and thermal camera (right).

Fig. 4. Raw natural color images from the UAS(left); accurate orthorectified mosaic image from EnsoMOSAIC (center); radiometric calibration of VIS image (right).

2.4. Data collection

The collection of the ground and remotely sensed data occurred under similar weather conditions in a one to two hour window.

2.4.1. Multispectral image acquisition

Four multispectral images were acquired by AggieAir during summer 2013. Acquisition dates were planned to coincide with different development stages and with overflights of Landsat. Images were collected, following the Landsat image acquisition protocol, close to solar noon (between 12 p.m. and 1 p.m.). The flight time (beginning to end) ranged from 30 to 40 min. All four missions were successfully performed, providing image data covering the earliest, middle, and latest periods of the oat growth. The spatial resolution is 0.15 m for VIS and NIR images and 0.6 m for the thermal infrared images.

2.4.2. Ground data acquisition

Intensive ground truth sampling of plant chlorophyll was conducted simultaneously with the AggieAir flights at precise GPS locations. The GPS data was collected using an rtkGPS with <1 mm precision in a 1 Hz bandwidth (Trimble® R8, Global Navigation Satellite System, Dayton, Ohio). A SPAD–502 chlorophyll meter (Minolta Corporation, New Jersey, USA) was used for in vivo measurement of the ratio of light transmittance through the leaf at wavelengths of 650 and 940 nm. Instrument readings have been shown to correlate well to laboratory measurements of chlorophyll concentration in several species (Yadawa, 1986). On each sampling campaign, 40 SPAD measurements were collected on average. The chlorophyll meter readings were taken midway on the fully expanded top-of-canopy leaves. Each measurement was characterized by the mean of six replicate measurements. The chlorophyll meter measures an area of 2×3 mm with an accuracy of ± 1.0 SPAD unit (at room temperature). However, the SPAD-502 meter displays the chlorophyll readings in arbitrary units (SPAD unit) rather than the actual amounts of chlorophyll in mass per leaf area; thus, further conversions were needed. The SPAD units were transformed to a Chlorophyll Concentration Index (CCI) unit using Eq. (8) and then to chlorophyll in mass per leaf area using Eq. (9) (Parry et al., 2014). Eq. (9) was developed for barley crops however, literature shows

Table 2
Statistical description of the dataset.

		Range	Mean ± SD
Potential Inputs	Blue	0.11–0.36	0.15 ± 0.04
	Green	0.20–0.49	0.26 ± 0.05
	Red	0.15–0.51	0.22 ± 0.07
	NIR	0.51–0.61	0.57 ± 0.02
	Thermal (°C)	23.11–36.16	29.88 ± 4.13
	NDVI	0–0.78	0.44 ± 0.12
	Green Model	0.17–1.74	1.17 ± 0.34
	LAI (m^2/m^2)	0–4.23	2.41 ± 0.90
Output	Chlorophyll ($\mu g\ cm^{-2}$)	0–61.64	47.01 ± 11.26

Table 3
Vegetative indices formulation.

Indices	Formula	Reference
Green model	$R_{NIR}/R_{Green} - 1$	(Gitelson et al., 2005)
NDVI	$(R_{NIR} - R_{red})/(R_{NIR} + R_{Red})$	(Rouse et al., 1974)
LAI[a]	$\ln[(NDVI\text{-}NDVI_{max})/(NDVI_{min} - NDVI_{max})]/-0.54$	(Smith et al., 2008; Duchemin et al., 2006)

[a] LAI was calculated empirically and not validated by field measurements.

that monocots have similar optical/absolute chlorophyll concentration relationship.

$$CCI = 1 + 0.00119 \times SPAD^{2.67} \quad (8)$$

$$Chlorophyll(\mu mol \times m^{-2}) = -132 + 146(CCI^{0.43}) \quad (9)$$

2.4.3. Linking on-ground measurements to airborne imagery

Ground coordinates of sampled chlorophyll coincided precisely with the location of the plants in the geo-rectified imagery. Ground coordinates of the samples were overlaid onto the geo-rectified imagery, and, using the ArcGIS spatial analyst tool (Extract Multi Values to Points), an automated process was developed to extract the pixel value representing the center of each sampled area.

2.5. Model potential inputs and performance

Three of the four flights (early growth, mid growth and early flowering), excluding the flight 10 days after planting, were used in the dataset to train and test the model. The dataset contains coincident in situ SPAD measurements used to derive chlorophyll concentration, and remote sensing reflectance measurements. All the data were collected from inside the center pivot quarter, the zeros found in the data set represent the areas of no vegetation (center pivot wheels trajectory). A statistical description of the dataset is presented in (Table 2). Each pair of data consists of a target, which is the chlorophyll concentration, and a set of 8 potential inputs tabulated in (Table 2). The potential inputs are composed of data retrieved form the UAS imagery (VIS, NIR, TIR), vegetative indices (Green model and NDVI) that were reported to be sensitive in estimating chlorophyll (Gitelson et al., 2005; Shanahan et al., 2003) and LAI, a well-known and widely used vegetation index related to crop growth. Table 3 shows the indices formulations.

These potential predictors, exert to a certain degree correlation between each other. This is because they are derived from the same AggieAir reflectance bands (statistical correlation). While in customary statistics (e.g., linear regression) using these predictors would raise issues, the Bayesian regression machine applied in this study can deal with this problem. The kernel or basis function projects these potential inputs into a higher dimensional space. The way these inputs are projected in the new dimensional space, as well as the sparse representation of the observations in the final model, help the model deal with collinearity issues.

In preliminary runs different potential inputs were explored. For example, one set composed of only single bands, and another set composed of the ratio of the single bands. In addition, the authors tried vegetative indices sensitive to chlorophyll estimations (TCARI, MCARI, and MTVI) that were modified to adapt to the spectral response of AggieAir sensors (e.g., replacing the required red edge by the NIR band). However, details on these preliminary runs are not reported in this study because of their low statistical performance.

The RVM is a well-established statistical learning algorithm that adopts a full probabilistic framework. Its key feature is that it can yield a solution function that depends on only a very small number of training samples (called relevance vectors). In the RVM framework, the model is built on the few training examples whose associated hyperparameters do not go to infinity during the training process, leading to a sparse solution. The implemented RVM is based on the MATLAB code provided via Michael E. Tipping's website. The RVM model in this research was first trained and tested using K-fold cross validation ($K = 5$); the cross validation technique is utilized to generalize an independent training data set (Kohavi, 1995). In this procedure, the training set is partitioned into K disjoint sets. The model is trained, for a chosen kernel, on all the subsets except for one, which is left for testing. The procedure is repeated for a total of K trials, each time using a different subset for testing. After the selection of the kernel function and its width, the whole data set is trained using RVM based regression. The advantage of this method over a random selection of training samples is that all observations are used for either training (K times) or evaluation (once).

The model was developed with an input selection process (Guyon and Elisseeff, 2003) in an attempt to explain the data in the simplest way possible. Potential inputs were examined to see which were most relevant to the target function and thus avoid degrading the performance of a learning algorithm due to the presence of irrelevant input variables. In each iteration, the input with the minimum efficiency was eliminated.

The RVM model was tested using six kernel types: Gauss, Laplace, spline, Cauchy, thin plate spline (tps), and bubble. The performance of the model was evaluated by comparing the root mean squared error (RMSE) and the Nash–Sutcliffe efficiency (E); these two parameters have been widely used to evaluate the performance of RVM models. The larger the value of E and the smaller the value of RMSE, the greater the precision and accuracy of the model to

predict chlorophyll. The RMSE and E are computed as shown in Eqs. (10) and (11), respectively:

$$\mathrm{RMSE} = \left[\sqrt{\frac{\sum_{t=1}^{N}(\hat{y}_t - y_t)^2}{N}}\right] \quad (10)$$

$$E = 1 - \frac{\sum_{t=1}^{N}(y_t - \hat{y})^2}{\sum_{t=1}^{N}(y_t - \bar{y})^2} \quad (11)$$

where, $\hat{y}_t$ = predicted chlorophyll concentration; y_t = measured chlorophyll concentration; $\bar{y}$ = mean of the observed chlorophyll concentration; $\bar{\hat{y}}$ = mean of the estimated chlorophyll concentration; and N = total number of observations.

3. Result and discussion

Each of the six kernel types was tested over a wide range of kernel widths (10^{-5}–10^{5}), and RMSE and E were calculated for all of the resulting models to assess their predictive capabilities. An embedded loop in the coding model was developed to represent the backward elimination tool. For each type of kernel and its corresponding width, the RVM was first run using all of the 8 inputs, consequently generating all of the needed statistical model performance estimates to assess the model. A set of defined iterations then eliminated, in order, the input with the minimum efficiency, thus removing the input least relevant to the target function. After numerous computational runs, four options presented themselves as potential "best model" scenarios (Table 4). All four of these potential "best model" scenarios had an RMSE <6 μg cm^{-2} and an E > 0.7. In 94% of all runs conducted across the six kernel types, the thermal band was the last input to be dropped, suggesting that thermal imagery is an important input, at least in the case of study area, possessing the most relevant information for estimating chlorophyll concentration. Thermal data allowed the models to differentiate between the bare soil and the different level of vegetation per pixel resulting in a more accurate chlorophyll estimates. A preliminary interpretation for that could be the fact that oat leaves are very thin, with minimal heat capacity and as a result, leaves exposed to full sunlight can warm up substantially above air temperature. This elevated temperature can help identify chlorophyll variability. Nevertheless, additional experiments that explore thermal imagery and its effect on chlorophyll estimations need to be conducted.

Table 4
Potential "best scenarios".

Model	Kernel type	# of Inputs	Inputs
1	Gaussian	4	LAI, NDVI, Thermal, Green
2	Gaussian	3	Thermal, Green, LAI
3	Laplace	4	NDVI, Red, green, Thermal
4	tps	4	LAI, NDVI, Thermal, Re

When plotting the 1-1 plot for the four best scenario candidates, the plots looked almost identical. Since the statistical performance does not reveal an absolute best model, visual comparison of the chlorophyll estimation maps of the four models, on one hand, and the NDVI, LAI, true-color maps on the other hand was conducted. The chlorophyll estimates for the early growth, mid growth, and early flowering images was developed considering the unique characteristic of each of the four best models (kernel type, width and set of inputs). Models 1 and 2 showed clear over-fitting when plotted over the entire map: in each case, the resulting map was one solid color, with no variation in estimated chlorophyll between bare soil and fully grown oat plants. Model 3 showed more variation within the field; nevertheless, visual comparisons with model 4 indicated that model 4 was superior. Model 4 showed an RSME of 5.31 μg cm^{-2}, an E of 0.76, and 9 relevance vectors. Fig. 5 illustrates the measured chlorophyll concentration versus estimated values with a one standard error confidence interval. The three flights are separated by the yellow line in the graph. Some differences can be

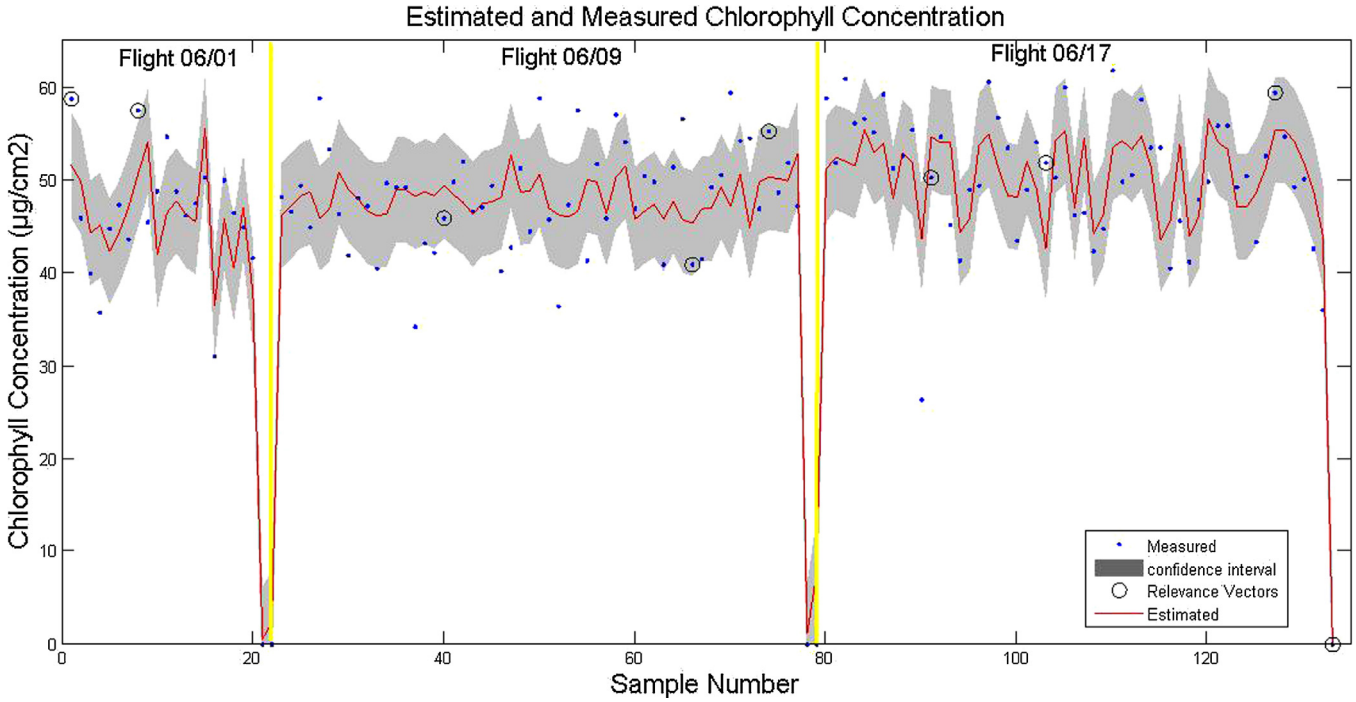

Fig. 5. Measured versus predicted chlorophyll concentration (μg cm^{-2}) in the three flights for model 4. Vertical yellow lines separates the three flight dates. (For interpretation of the references to color in this figure legend, the reader is referred to the web version of this article.)

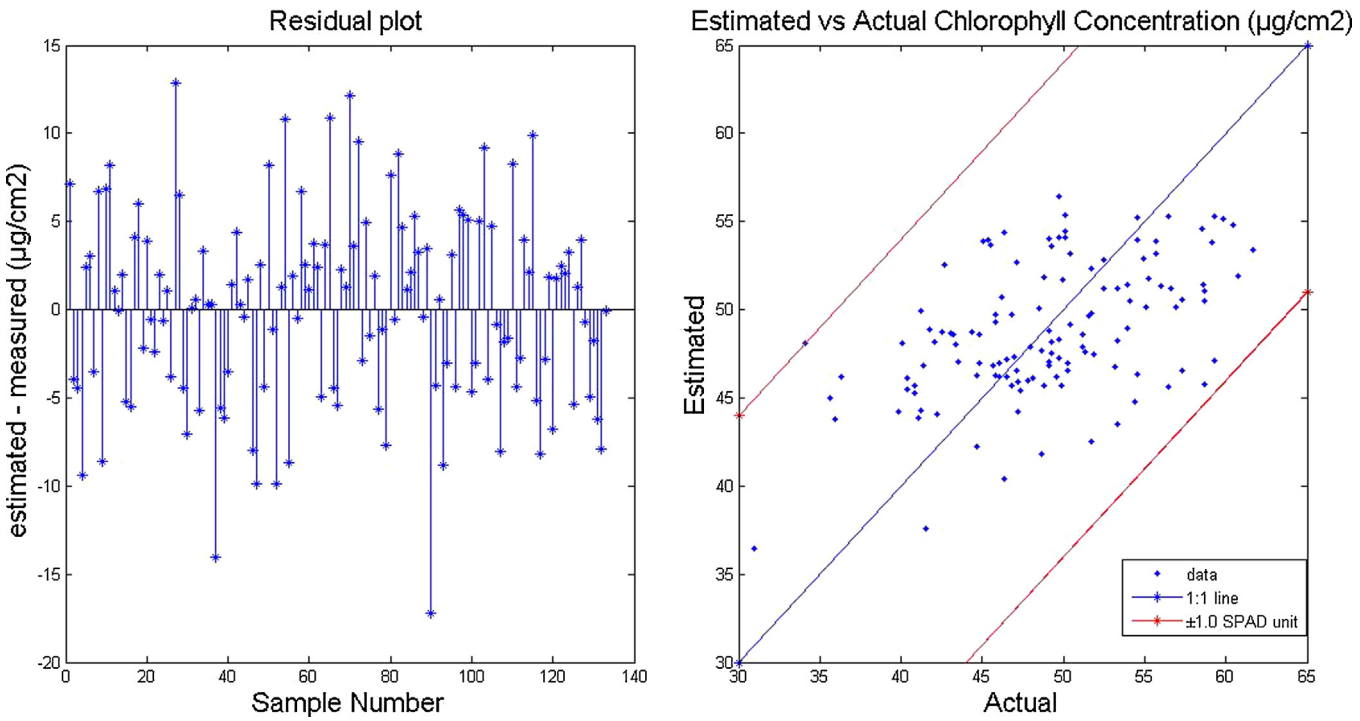

Fig. 6. Model 4: Residual plot of the three flights (left) and one-by-one plot excluding the bare soil–zero chlorophyll points and reflecting the chlorophyll meter accuracy (right).

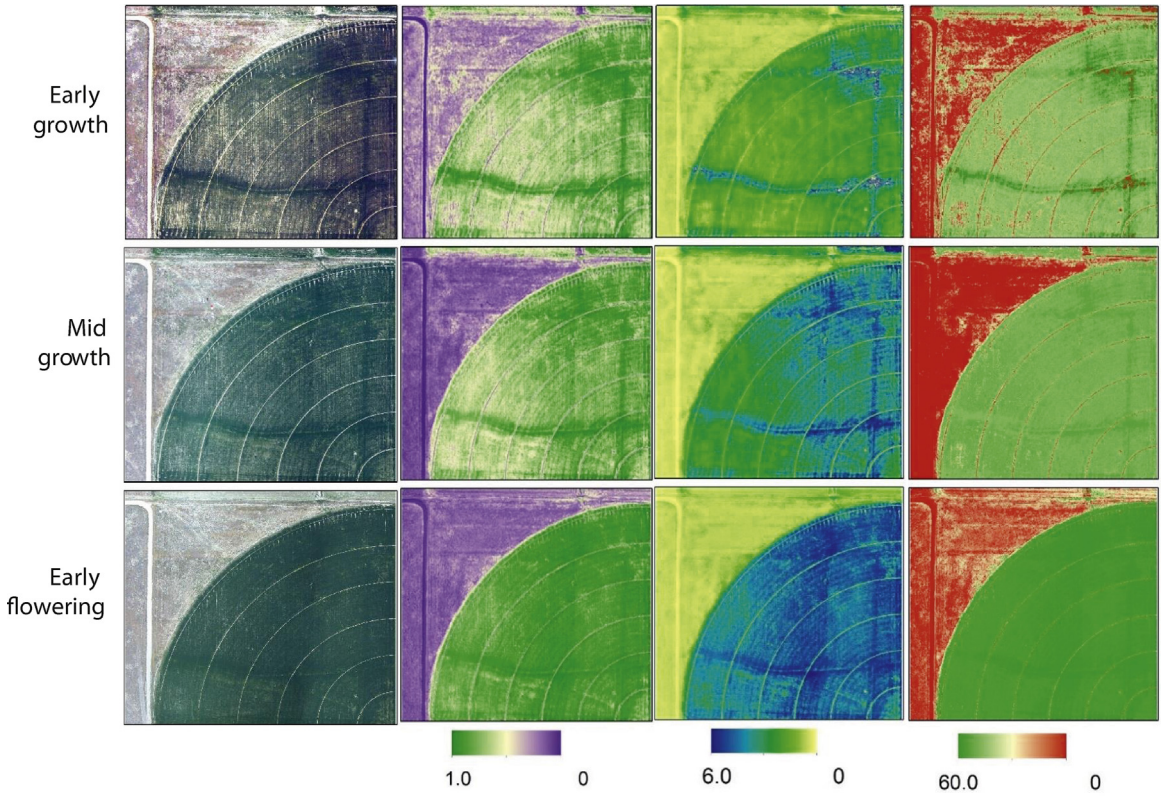

Fig. 7. True color maps, NDVI maps, LAI maps (m^2/m^2) and the estimated chlorophyll concentration ($\mu g\,cm^{-2}$) map, for the three different dates representing early growth, mid growth and early flowering.

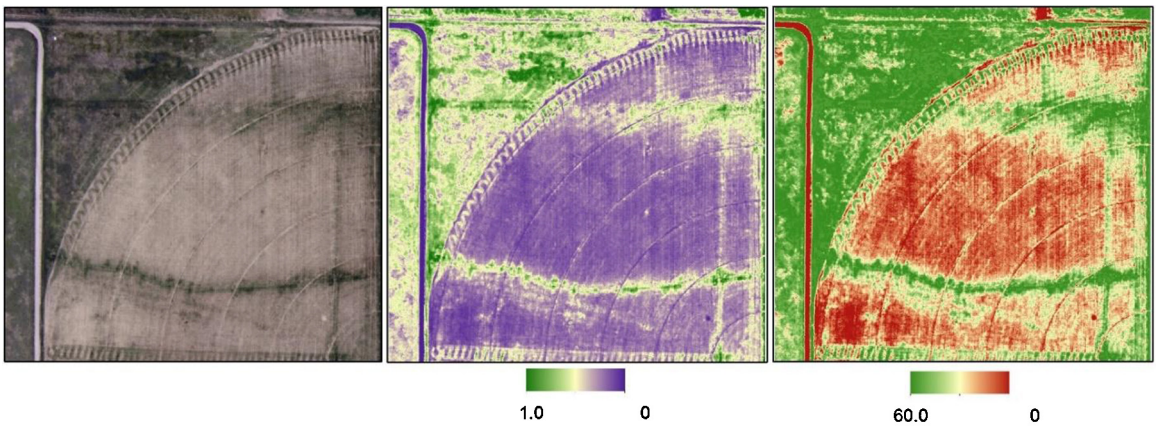

Fig. 8. True color image of May 16 flight (left), NDVI map (middle), and estimated chlorophyll concentration map ($\mu g\,cm^{-2}$) (right).

observed between the different dates, the estimates for the first and third flights are more precise than the second flight. This could be due to the stage of the crop growth or the homogeneity of the vegetation cover.

Fig. 6 represents regression diagnostic plots of model 4 that address model assumptions like linearity and equality of variances. The 1:1 plot confirms the adequacy of the model proposed for most of the chlorophyll values lying within the boundaries of ± 1.0 SPAD unit (sensor accuracy), which corresponds to 14 $\mu g\,cm^{-2}$. The chlorophyll maps generated from model 4, along with NDVI and LAI, are presented in Fig. 7.

As shown in Fig. 7, the predicted chlorophyll concentration maps show a visual good agreement with the LAI and NDVI maps. In the early growth image, the field exterior had weeds growing in it, which explains the predicted chlorophyll concentration values. This area was not irrigated during the growing cycle, leaving the weeds to dry and senescence, thus, a near zero chlorophyll concentration value was assigned by the model in the following two images. Also, the wheel tracks and the access road that are located around the center pivot had no vegetation cover, and the model successfully assigned a near zero chlorophyll concentration to these features. Another common pattern was the two thick horizontal and vertical lines that protrude in the images. These were past ditch lines that had been used in flood irrigation activities prior to the conversion of the field to a center pivot system. The greater water content in those areas caused the plants growing along those two lines to be very vigorous. This is reflected in the high chlorophyll concentration values given to the plants in this area.

Chlorophyll concentration varies widely within the growing season, therefore any recommended analytical technique must perform well under unseen data. To explore the model with unseen data, May 16 flight was used. Now that the model is established with a defined set of features (inputs, kernel type, kernel width...) May 16 flight (10 days after planting of the oats) is entered in the model to explore the models performance when subjected to totally unseen data. The predicted chlorophyll concentration map is shown in Fig. 8.

Again, the predicted chlorophyll concentration map for the fourth flight showed good association with the NDVI map. Areas of vigorous growth, bare soil, and low vegetation were similar in the three maps and represented similar growth patterns. This test reported an RSME of 8.52 $\mu g\,cm^{-2}$ and E of 0.71 for this flight. This result showed that the model successfully performed when given unseen data.

Despite the complexity of the statistical model included in this paper, it is anticipated that the lucid output (chlorophyll concentration maps) will help agricultural decision makers quantify field chlorophyll and address its variability and as a result improve input efficiency, environmental sustainability and yield. Adoption of precision agriculture is likely to continue into the foreseeable future. However, studies that explores high-resolution sensors (<1 m) with adequate frequent coverage, combined with techniques capable of extracting information from imagery to provide near real time information will be a determining factor in the adoption rate of precision agriculture.

4. Conclusion

This paper presented the application of imagery from AggieAir a remote sensing platform, combined with machine learning algorithms (RVM) to estimate chlorophyll concentration as an important biophysical parameter to be used in precision agriculture. The RVM modeling technique, coupled with cross validation and backward elimination, was applied to a data set composed of reflectance from high-resolution multi-spectral imagery (VIS–NIR), thermal infrared imagery, and vegetative indices, in conjunction with in situ chlorophyll concentrations derived from SPAD measurements. Six kernel types were tested over a wide range of kernel widths. Model performance was evaluated by comparing the RMSE and E of various models and later by visual comparison. Chlorophyll concentration estimation was best achieved with Model 4 (kernel type: thin plate spline; kernel width: 5.4; selected inputs: LAI, NDVI, thermal and red band; RSME: 5.31 $\mu g\,cm^{-2}$; E: 0.76; and 9 relevance vectors) for the three flights. Of all the inputs, thermal band was retained last in 94% of the models, proving the significance of thermal imagery as an input possessing the most relevant information in estimating chlorophyll concentration.

Converting these chlorophyll estimate maps into actionable information to benefit the end user now shows promise. Other research that estimates soil moisture, actual evapotranspiration, and soil nutrient content using the same high resolution aerial platforms allows for wider adoption of precision agriculture by future farmers. Although the results presented in this section are arguably not yet actionable, maps like these could be used to quantify plant health, predict yield, and indicate where and how much fertilizer to apply.

AggieAir imagery, combined with appropriate analytic tools, allows spatial estimation of chlorophyll concentration. These estimates, made at such fine resolutions in space and time, can aid farmers in assessing the heterogeneity of their fields and subsequently implement needed actions accordingly. The high-resolution spatial information generated from AggieAir imagery could enable far greater precision in the application of nitrogen fertilizers and identification of stressed crops.

Acknowledgments

This research was supported by the Utah Water Research Laboratory (UWRL), the Provo/Utah Office of the US Bureau of Reclamation, and the AggieAir Flying Circus at the UWRL. The authors appreciate the support of the USU AggieAir team that helped in the data collection procedure. Special thanks goes to the Division of Research Computing in the Office of Research (DoRC) at USU. Appreciation goes to Mrs. Carri Richards for her timely help in editing the paper. The authors thank the editor and the anonymous reviewers for their valuable comments that helped improving this paper.

References

Bachour, R., Walker, W., Ticlavilca, A., McKee, M., Maslova, I., 2014. Estimation of spatially distributed evapotranspiration using remote sensing and a relevance vector machine. J. Irrig. Drain. Eng. 140 (8), 4014029.

Bauer, M.E., 1985. Spectral inputs to crop identification and condition assessment. Proc. IEEE 73 (6), 1071–1085.

Baret, F., Buis, S., 2008. Estimating canopy characteristics from remote sensing observations: review of methods and associated problems. In: Inadvances in Land Remote Sensing. Springer Netherlands, pp. 173–201.

Benedetti, R., Rossini, P., 1993. On the use of NDVI profiles as a tool for agricultural statistics: the case study of wheat yield estimate and forecast in *Emilia Romagna*. Remote Sens. Environ. 45 (3), 311–326.

Bernie, J., Zarco-Tejada, P.J., Suárez, L., Fereres, E., 2009. Thermal and narrowband multispectral remote sensing for vegetation monitoring from an unmanned aerial vehicle. IEEE Trans. Geosci. Remote Sens. 47 (3), 722–738.

Berry, J., Bjorkman, O., 1980. Photosynthetic response and adaptation to temperature in higher plants. Annu. Rev. Plant Physiol. 31 (1), 491–543.

Blackburn, G.A., 1998. Quantifying chlorophylls and caroteniods at leaf and canopy scales: an evaluation of some hyperspectral approaches. Remote Sens. Environ. 66 (3), 273–285.

Blum, A., Mayer, J., Gozlan, G., 1982. Infrared thermal sensing of plant canopies as a screening technique for dehydration avoidance in wheat. Field Crops Res. 5, 137–146.

Brisco, B., Brown, R.J., Hirose, T., McNairn, H., Staenz, K., 1998. Precision agriculture and the role of remote sensing: a review. Can. J. Remote Sens. 24 (3), 315–327.

Bonge, N.H., Leblanc, E., 2001. Comparing prediction power and stability of broadband and hyperspectral vegetation indices for estimation of green leaf area index and canopy chlorophyll density. Remote Sens. Environ. 76 (2), 156–172.

Camps-Valls, G., Bruzzone, L., Rojo-Álvarez, J.L., Melgani, F., 2006. Robust support vector regression for biophysical variable estimation from remotely sensed images. Geosci. Remote Sens. Lett. IEEE 3 (3), 339–343.

Camps-Valls, G., Gómez-Chova, L., Muñoz-Marí, J., Vila-Francés, J., Amorós-López, J., Calpe-Maravilla, J., 2006b. Retrieval of oceanic chlorophyll concentration with relevance vector machines. Remote Sens. Environ. 105 (1), 23–33.

Carter, G.A., Spiering, B.A., 2002. Optical properties of intact leaves for estimating chlorophyll concentration. J. Environ. Qual. 31 (5), 1424–1432.

Chaerle, L., Van Der Straeten, D., 2000. Imaging techniques and the early detection of plant stress. Trends Plant Sci. 5 (11), 495–501.

Cipollini, P., Corsini, G., Diani, M., Grasso, R., 2001. Retrieval of sea water optically active parameters from hyperspectral data by means of generalized radial basis function neural networks. IEEE Trans. Geosci. Remote Sens. 39 (7), 1508–1524.

Clemens, S.R., (2012). Procedures for Correcting Digital Camera Imagery Acquired by the AggieAir Remote Sensing Platform, Utah State University, 2012.

N., Cristianini, J., Shawe-Taylor, An introduction to support vector machines and other kernel-based learning methods, Cambridge university press, 2000.

Crowther, B.G., (1992). Radiometric calibration of multispectral video imagery (Doctoral dissertation, Utah State University. Department of biological and Irrigation Engineering).

Daberkow, S.G., McBride, W.D., Robert, P.C., Rust, R.H., Larson, W.E., 2000. Adoption of precision agriculture technologies by US farmers. Bloomington, Minnesota, USA In: Proceedings of the 5th International Conference on Precision Agriculture, 16–19 July, pp. 1–12, American Society of Agronomy.

Datt, B., 1999. A new reflectance index for remote sensing of chlorophyll content in higher plants: tests using eucalyptus leaves. J. Plant Physiol. 154 (1), 30–36.

Daughtry, C.S.T., Walthall, C.L., Kim, M.S., De Colstoun, E.B., McMurtrey Iii, J.E., 2000. Estimating corn leaf chlorophyll concentration from leaf and canopy reflectance. Remote Sens. Environ. 74 (2), 229–239.

Dawson, T.P., North, P.R.J., Plummer, S.E., Curran, P.J., 2003. Forest ecosystem chlorophyll content: implications for remotely sensed estimates of net primary productivity. Int. J. Remote Sens. 24 (3), 611–617.

De Martino, M., Mantero, P., Serpico, S.B., Carta, E., Corsini, G., Grasso, R., 2002. Water quality estimation by neural networks based on remotely sensed data analysis. Proc. of the International Workshop on Geo-spatial Knowledge Processing for Natural Resource Management, 54–58.

Demarez, V., Gastellu-Etchegorry, J.P., 2000. A modeling approach for studying forest chlorophyll content. Remote Sens. Environ. 71 (2), 226–238.

Demir, B., Erturk, S., 2007. Hyperspectral image classification using relevance vector machines. Geosci. Remote Sens. Lett. IEEE 4 (4), 586–590.

Duchemin, B., Hadria, R., Erraki, S., Boulet, G., Maisongrande, P., Chehbouni, A., Simonneaux, V., 2006. Monitoring wheat phenology and irrigation in Central Morocco: on the use of relationships between evapotranspiration crops coefficients leaf area index and remotely-sensed vegetation indices. Agric. Water Manage. 79 (1), 1–27.

Evans, J.R., 1989. Photosynthesis and nitrogen relationships in leaves of C3 plants. Oecologia 78 (1), 9–19.

Franke, J., Menz, G., 2007. Multi-temporal wheat disease detection by multi-spectral remote sensing. Precis. Agric. 8 (3), 161–172.

Genton, M.G., 2002. Classes of kernels for machine learning: a statistics perspective. J. Mach. Learn. Res. 2, 299–312.

Gitelson, A., Merzlyak, M.N., 1994. Quantitative estimation of chlorophyll a using reflectance spectra: experiments with autumn chestnut and maple leaves. J. Photochem. Photobiol. B 22 (3), 247–252.

Gitelson, A.A., Kaufman, Y.J., Merzlyak, M.N., 1996. Use of a green channel in remote sensing of global vegetation from EOS-MODIS. Remote Sens. Environ. 58 (3), 289–298.

Gitelson, A.A., Vina, A., Ciganda, V., Rundquist, D.C., Arkebauer, T.J., 2005. Remote estimation of canopy chlorophyll content in crops. Geophys. Res. Lett. 32 (8).

Gitelson, A.A., Viña, A., Verma, S.B., Rundquist, D.C., Arkebauer, T.J., Keydan, G., Suyker, A.E., 2006. Relationship between gross primary production and chlorophyll content in crops: implications for the synoptic monitoring of vegetation productivity. J. Geophys. Res. 1984–2012 (111), D8.

Gómez-Chova, L., Muñoz-Marí, J., Laparra, V., Malo-López, J., Camps-Valls, G., 2011. A review of kernel methods in remote sensing data analysis. In: In Optical Remote Sensing, Springer Berlin Heidelberg, pp. 171–206.

González Vilas, L., Spyrakos, E., Torres Palenzuela, J.M., 2011. Neural network estimation of chlorophyll a from MERIS full resolution data for the coastal waters of galician rias (NW Spain). Remote Sens. Environ. 115 (2), 524–535.

Guyon, I., Elisseeff, A., 2003. An introduction to variable and feature selection. J. Mach. Learn. Res. 3, 1157–1182.

Haboudane, D., Miller, J.R., Tremblay, N., Zarco-Tejada, P.J., Dextraze, L., 2002. Integrated narrow-band vegetation indices for prediction of crop chlorophyll content for application to precision agriculture. Remote Sens. Environ. 81 (2), 416–426.

Haboudane, D., Miller, J.R., Pattey, E., Zarco-Tejada, P.J., Strachan, I.B., 2004. Hyperspectral vegetation indices and novel algorithms for predicting green LAI of crop canopies: modeling and validation in the context of precision agriculture. Remote Sens. Environ. 90 (3), 337–352.

Hassan Esfahani, L., Torres-Rua, A., Jensen, A., McKee, M., (2014). Top soil moisture estimation for precision agriculture using unmmaned aerial vehicle multispectral imagery, Geoscience and Remote Sensing Symposium (IGARSS), 2014 IEEE International.

Hassan Esfahani, L., Torres-Rua, A., Jensen, A., McKee, M., 2014b. Assessment of surface soil moisture using high-resolution multi-spectral imagery and artificial neural networks. Remote Sens., 2015.

Hastie, T., Tibshirani, R., Friedman, J., Hastie, T., Friedman, J., Tibshirani, R., 2009. The elements of statistical learning, Vol. 2. Springer, New York (No. 1).

Idso, S.B., Jackson, R.D., Reginato, R.J., 1977. Remote-sensing of crop yields. Science 196 (4285), 19–25.

Infrared Cameras Incorporated, http://www.infraredcamerasinc.com, 2012.

Jackson, Idso, S.B., Reginato, R.J., Pinter, P.J., 1981. Canopy temperature as a crop water stress indicator. Water Resour. Res. 17 (4), 1133–1138.

Jackson, R.D., (1984, October). Remote sensing of vegetation characteristics for farm management, In 1984 Technical Symposium East (pp. 81-97), International Society for Optics and Photonics.

Jensen, A.M., 2014. Innovative payloads for small unmanned aerial system-based personal remote sensing and applications. PhD thesis. In: Department of Electrical & Computer Engineering. Logan, UT, Utah State University.

Jiang, J., Liu, D., Gu, J., Susstrunk, S., (2013, January). What is the space of spectral sensitivity functions for digital color cameras? In Applications of Computer Vision (WACV), 2013 IEEE Workshop on (pp. 168-179). IEEE.

Johnson, L.F., Hlavka, C.A., Peterson, D.L., 1994. Multivariate analysis of AVIRIS data for canopy biochemical estimation along the Oregon transect. Remote Sens. Environ. 47 (2), 216–230.

Kalluri, S., Gilruth, P., Bergman, R., Plante, R., (2002, June). Impacts of NASA's remote sensing data on policy and decision making at state and local agencies in the United States, In Geoscience and Remote Sensing Symposium, 2002, IGARSS'02, 2002 IEEE International (Vol. 3, pp. 1691-1693), IEEE.

Kim, M.S., 1994. The use of narrow spectral bands for improving remote sensing estimation of fractionally absorbed photosynthetically active radiation (fAPAR). In: Masters Thesis, Department of Geography. College Park, MD, University of Maryland.

Kim, M.S., Daughtry, C.S.T., Chappelle, E.W., McMurtrey III, J.E., Walthall, C.L., 1994. The use of high spectral resolution bands for estimating absorbed photosynthetically active radiation (Apar). Val D'Isere, France In: Proceedings of the 6th Symposium on Physical Measurements and Signatures in Remote Sensing, January 17–21, pp. 299–306.

Knudby, A., LeDrew, E., Brenning, A., 2010. Predictive mapping of reef fish species richness, diversity and biomass in zanzibar using IKONOS imagery and machine-learning techniques. Remote Sens. Environ. 114 (6), 1230–1241.

Kohavi, R., 1995 August. A study of cross-validation and bootstrap for accuracy estimation and model selection. In IJCAI Vol. 14, 1137–1145, No. 2.

Lamb, D.W., Brown, R.B., 2001. PA—precision agriculture: remote-sensing and mapping of weeds in crops. J. Agric. Eng. Res. 78 (2), 117–125.
Lambert, D., Lowenberg-De Boer, J., (2000). Precision agriculture profitability review, Purdue University, http://agriculture.purdue.edu/SSMC/Frames/newsoilsX.pdf
Le Maire, G., Francois, C., Dufrene, E., 2004. Towards universal broad leaf chlorophyll indices using PROSPECT simulated database and hyperspectral reflectance measurements. Remote Sens. Environ. 89 (1), 1–28.
Liaghat, S., Balasundram, S.K., 2010. A review: the role of remote sensing in precision agriculture. Am. J. Agric. Biol. Sci. 5 (1), 50.
MacDonald, R.B., Hall, F.G., 1980. Global crop forecasting. Science 208 (4445), 670–679.
Mathur, A., Foody, G.M., 2008. Crop classification by support vector machine with intelligently selected training data for an operational application. Int. J. Remote Sens. 29 (8), 2227–2240.
Miller, J.R., Hare, E.W., Wu, J., 1990. Quantitative characterization of the vegetation red edge reflectance 1. An inverted-gaussian reflectance model. Remote Sens. 11 (10), 1755–1773.
Miura, T., Huete, A.R., 2009. Performance of three reflectance calibration methods for airborne hyperspectral spectrometer data. Sensors 9 (2), 794–813.
Moran, M.S., Inoue, Y., Barnes, E.M., 1997. Opportunities and limitations for image-based remote sensing in precision crop management. Remote Sens. Environ. 61 (3), 319–346.
Moran, J.A., Mitchell, A.K., Goodmanson, G., Stockburger, K.A., 2000. Differentiation among effects of nitrogen fertilization treatments on conifer seedlings by foliar reflectance: a comparison of methods. Tree Physiol. 20 (16), 1113–1120.
MosaicMill Oy, EnsoMOSAIC Image Processing User's Guide. Version 7.3. Mosaic Mill Ltd. Finland, 2009.
Moser, G., Serpico, S.B., 2009. Automatic parameter optimization for support vector regression for land and sea surface temperature estimation from remote sensing data. IEEE Trans. Geosci. Remote Sens. 47 (3), 909–921.
Murakami, Y., Tsuyama, M., Kobayashi, Y., Kodama, H., Iba, K., 2000. Trienoic fatty acids and plant tolerance of high temperature. Science 287 (5452), 476–479.
Myneni, R.B., Maggion, S., Iaquinta, J., Privette, J.L., Gobron, N., Pinty, B., Williams, D.L., 1995. Optical remote sensing of vegetation: modeling, caveats, and algorithms. Remote Sens. Environ. 51 (1), 169–188.
Neale, C.M., Crowther, B.G., 1994. An airborne multispectral video/radiometer remote sensing system: development and calibration. Remote Sens. Environ. 49 (3), 187–194.
Niinemets, Ü., Tenhunen, J.D., 1997. A model separating leaf structural and physiological effects on carbon gain along light gradients for the shade-tolerant species *Acer saccharum*. Plant Cell Environ. 7, 845–866.
Pal, M., Mather, P.M., 2005. Support vector machines for classification in remote sensing. Int. J. Remote Sens. 26 (5), 1007–1011.
Parry, C., Blonquist, J., Bugbee, B., 2014. In situ measurement of leaf chlorophyll concentration: analysis of the optical/absolute relationship. Plant Cell Environ.
Peñuelas, J., Filella, I., 1998. Visible and near-infrared reflectance techniques for diagnosing plant physiological status. Trends Plant Sci. 3 (4), 151–156.
Pierce, F.J., Nowak, P., 1999. Aspects of precision agriculture. Adv. Agron. 67, 1–85.
Raison, J.K., Roberts, J.K., Berry, J.A., 1982. Correlations between the thermal stability of chloroplast (thylakoid) membranes and the composition and fluidity of their polar lipids upon acclimation of the higher plant, *Nerium oleander*, to growth temperature. Biochim. Biophys. Acta 688 (1), 218–228.
Rouse, J.W., Haas, R.H., Schell, J.A., Deering, D.W., Harlan, J.C., (1974). Monitoring the vernal advancements and retrogradation of natural vegetation in Nasa, Gsfc final report (ed. MD, UG) p, 1-371.
Salvucci, M.E., Crafts-Brandner, S.J., 2004. Inhibition of photosynthesis by heat stress: the activation state of rubisco as a limiting factor in photosynthesis. Physiol. Plant. 120 (2), 179–186.
Schellberg, J., Hill, M.J., Gerhards, R., Rothmund, M., Braun, M., 2008. Precision agriculture on grassland: applications, perspectives and constraints. Eur. J. Agron. 29 (2), 59–71.
Seelan, S.K., Laguette, S., Casady, G.M., Seielstad, G.A., 2003. Remote sensing applications for precision agriculture: a learning community approach. Remote Sens. Environ. 88 (1), 157–169.
Shanahan, J.F., Schepers, J.S., Francis, D.D., Varvel, G.E., Wilhelm, W.W., Tringe, J.M., Major, D.J., 2001. Use of remote-sensing imagery to estimate corn grain yield. Agron. J. 93 (3), 583–589.
Shanahan, J.F., Holland, K.H., Schepers, J.S., Francis, D.D., Schlemmer, M.R., Caldwell, R., 2003. Use of a crop canopy reflectance sensor to assess corn leaf chlorophyll content. Digital Imaging Spectral Techn., 135–150.
Sharkey, T.D., 2005. Effects of moderate heat stress on photosynthesis: importance of thylakoid reactions, rubisco deactivation, reactive oxygen species, and thermos tolerance provided by isoprene. Plant Cell Environ. 28 (3), 269–277.
Sims, D.A., Gamon, J.A., 2002. Relationships between leaf pigment content and spectral reflectance across a wide range of species, leaf structures and developmental stages. Remote Sens. Environ. 81 (2), 337–354.
Smith, A.M., Bourgeois, G., Teillet, P.M., Freemantle, J., Nadeau, C., 2008. A comparison of NDVI and MTVI2 for estimating LAI using CHRIS imagery: a case study in wheat. Can. J. Remote Sens. 34 (6), 539–548.
Souza, C.R., Kernel Functions for Machine Learning Applications, 17 Mar. 2010. Web. http://crsouza.blogspot.in/2010/03/kernel-functions-for-machine-learning.html
Stone, M.L., Solie, J.B., Raun, W.R., Whitney, R.W., Taylor, S.L., Ringer, J.D., 1996. Use of spectral radiance for correcting in-season fertilizer nitrogen deficiencies in winter wheat. Trans. ASAE 39 (5), 1623–1631.
Swinton, S.M., Lowenberg-DeBoer, J., 1998. Evaluating the profitability of site-specific farming. J. Prod. Agric. 11 (4), 439–446.
Thayananthan, A., Navaratnam, R., Stenger, B., Torr, P.H., Cipolla, R., 2008. Pose estimation and tracking using multivariate regression. Pattern Recognit. Lett. 29 (9), 1302–1310.
Ticlavilca, A.M., McKee, M., Walker, W.R., 2013. Real-time forecasting of short-term irrigation canal demands using a robust multivariate bayesian learning model. Irrigation Sci. 31 (2), 151–167.
Tipping, M.E., 2001. Sparse bayesian learning and the relevance vector machine. J. Mach. Learn. Res. 1, 211–244.
Tipping, M.E., 2004. Bayesian inference: an introduction to principles and practice in machine learning. In: In Advanced lectures on machine Learning, Springer Berlin Heidelberg, pp. 41–62.
Tipping, M.E., Faul, A.C., 2003 January. Fast marginal likelihood maximisation for sparse Bayesian models. In Proceedings of the ninth international workshop on artificial intelligence and statistics Vol. 1, No. 3.
Torres, A.F., Walker, W.R., McKee, M., 2011. Forecasting daily potential evapotranspiration using machine learning and limited climatic data. Agric. Water Manag. 98 (4), 553–562.
V., Vapnik, The nature of statistical learning theory, Springer Science & Business Media, 2000.
Verrelst, J., Schaepman, M.E., Malenovský, Z., Clevers, J.G., 2010. Effects of woody elements on simulated canopy reflectance: implications for forest chlorophyll content retrieval. Rem. Sens. Environ. 114 (3), 647–656.
Verrelst, J., Alonso, L., Camps-Valls, G., Delegido, J., Moreno, J., 2012. Retrieval of vegetation biophysical parameters using gaussian process techniques. IEEE Trans. Geosci. Remote Sens. 50 (5), 1832–1843.
Wallace, L., Lucieer, A., Watson, C., Turner, D., 2012. Development of a UAV-LiDAR system with application to forest inventory. Remote Sens. 4 (6), 1519–1543.
Weis, E., 1981. Reversible heat-inactivation of the calvin cycle: a possible mechanism of the temperature regulation of photosynthesis. Planta 151 (1), 33–39.
Wood, C.W., Tracy, P.W., Reeves, D.W., Edmisten, K.L., 1992. Determination of cotton nitrogen status with a handheld chlorophyll meter. J. Plant Nutr. 15 (9), 1435–1448.
Yadawa, U.L., 1986. A rapid and nondestructive method to determine chlorophyll in intact leaves. HortScience 21 (6), 1449–1450.
Yoder, B.J., Pettigrew-Crosby, R.E., 1995. Predicting nitrogen and chlorophyll content and concentrations from reflectance spectra (400–2500 nm) at leaf and canopy scales. Remote Sens. Environ. 53 (3), 199–211.
Yuan, J., Wang, K., Yu, T., Fang, M., 2007. Integrating relevance vector machines and genetic algorithms for optimization of seed-separating process. Eng. Appl. Artif. Intell. 20 (7), 970–979.
Zaman, B., Jensen, A., Clemens, S.R., McKee, M., 2014. Retrieval of spectral reflectance of high resolution multispectral imagery acquired with an autonomous unmanned aerial vehicle. Photogramm. Eng. Remote Sens. 80 (12), 1139–1150.
Zarco-Tejada, P.J., Miller, J.R., 1999. Land cover mapping at BOREAS using red edge spectral parameters from CASI imagery. J. Geophys. Res. 27, 27921–27933.
Zarco-Tejada, P.J., Miller, J.R., Noland, T.L., Mohammed, G.H., Sampson, P.H., 2001. Scaling-up and model inversion methods with narrowband optical indices for chlorophyll content estimation in closed forest canopies with hyperspectral data. IEEE Trans. Geosci. Remote Sens. 39 (7), 1491–1507.
Zarco-Tejada, P.J., Miller, J.R., Morales, A., Berjón, A., Agüera, J., 2004. Hyperspectral indices and model simulation for chlorophyll estimation in open-canopy tree crops. Remote Sens. Environ. 90 (4), 463–476.